(Received 18 May 2026, Accepted 3 July 2026, Scheduled 13 August 2026)

Effects of Cylindrical and Conical Conformal Bending on a Flexible Cylindrical Dielectric Resonator Antenna for X-Band Applications

Amera Anjum* and Jagadish C. Mudiganti

School of Electronics Engineering, VIT-AP University, Amaravati, India

ABSTRACT: Growing demand for conformal, on-body communication systems has driven the development of compact, mechanically flexible, and conformal antennas. However, the reported literature on flexible dielectric resonator antennas with systematic conformal analysis is limited. This research gap has motivated the present investigations. The study aims to assess the comprehensive conformal analysis of a flexible cylindrical dielectric resonator antenna (CDRA) designed for X-band (operating near 10 GHz). The proposed antenna is bent over cylindrical and conical surfaces with radii of 40 mm and 30 mm, respectively. The conformal configurations are analyzed to evaluate performance and subsequently validated through experiments. The planar antenna resonates at 10.5 GHz, with a measured gain of approximately 5.2 dBi and a bandwidth of 450 MHz (10.27–10.72 GHz). The simulated results showed a downward frequency shift for both cylindrical and conical bending environments compared to the planar configuration. At the same time, the prototype measurements demonstrated an upward shift in the frequency of cylindrical bending of the antenna with increasing curvature, due to material-dependent properties. In contrast, the antenna undergoes nonuniform geometric deformation and strain-dependent permittivity behavior during conical bending. This leads to a downward shift in frequency and significant variations in radiation characteristics. Despite deformations, a stable broadside radiation performance and practically viable gain levels were achieved, with an overall bandwidth of 10.26–11.2 GHz. In addition, a specific absorption rate (SAR) analysis confirms the antenna's compliance with general public exposure safety limits, with a maximum SAR peak of 1.26 W/kg for 10 g averaged mass, in accordance with safety standards. The conformal analyses, along with SAR validation for compact (less than 2 mm) and fully flexible CDRA, substantiate the novelty of the present study. Hence, the proposed antenna maintains a reliable performance under various bending conditions, highlighting its suitability for flexible, conformal, and wearable X-band applications.

1. INTRODUCTION

Over time, technological developments have led to significant advances in wireless communication systems to meet the requirements of advanced connecting devices. In such a scenario, antennas play a vital role in connecting devices and enabling communication to perform a specific task. To date, various antennas have been proposed for both low- and high-frequency applications. For integrated modules, deploying metallic patch antennas became more preferable. Moreover, to achieve high-speed point-to-point communication, it is most desirable for transmitter and receiver antennas to connect efficiently by adapting the surface of any prescribed integrated shape.

The ease of conformal integration of metal to various geometries has led to the development of non-planar metal antennas. Thus, non-planar antennas have emerged as more beneficial in terms of mechanical stability, reduced protrusion, and improved radiation characteristics, such as maximum angular coverage, when mounted or wrapped over non-planar (curved) surfaces, as compared to planar antennas.

An antenna that conforms to the surface upon which it is mounted or integrated without causing extra drag is called a conformal antenna (CA). Curved surfaces, such as cylindrical, conical, spherical, or other crumpled geometry, can define the antenna's shape. Conformal antennas were developed mainly for aircraft (non-planar surfaces) applications due to their less protruding feature [1, 2]. Currently, conformal antennas are used in mobile communication, navigation systems, medicine, intelligent devices, airborne vehicles, real-time tracking systems, and military applications.

The radiating element varies along the curvature of smooth surfaces in conformal antennas. Unlike planar surfaces, non-planar geometries exhibit variation with respect to radial (ρ), azimuthal (φ), and elevation (θ) directions. In the case of a cylindrical surface, a variation occurs along the azimuthal (φ) direction. The conical surface undergoes radial (ρ) and azimuthal (φ) variations. Similarly, a spherical surface follows deviation in radial (ρ), azimuthal (φ), and elevation (θ) directions [3].

Based on different substrates, many metal patch antennas and arrays have been reported since the beginning of the conformal antenna era. The numerical analyses of antennas' near-field and far-field characteristics have been explored and compared

* Corresponding author: Amera Anjum (amera.anjum@vitap.ac.in).

with those of planar patch antennas. Microstrip lines, coaxial, aperture-coupled, and proximity-coupled are the feeding techniques used to excite the antenna. The upward or downward shift in resonant frequency, a reduction in antenna gain, and a slightly distorted radiation pattern result from bending the antenna over non-planar surfaces [4–6].

The conformal antenna can be flexible or non-flexible depending on its deployment. A flexible antenna (FA) deforms easily on any mounting or integrating surface, unlike a non-flexible antenna, which bends only on a predefined surface. For decades, conformal antennas were rigid because flexible substrates were unavailable. In recent years, the development of flexible materials that withstand deformation and remain mechanically reliable has led to a revolution in the design of flexible, conformal antennas [7].

The demand for compact, lightweight, flexible devices has necessitated the investigation of flexible substrates. Flexible substrates offer advantages in terms of elasticity, deformability, and durability compared to non-flexible substrates. With the advent of flexible materials, the electronics industry has witnessed tremendous growth, and production may continue to increase in the long run [8, 9]. Today, flexible substrates are used in high-speed electronic devices, medical devices, sensors, displays, energy storage devices, and antennas.

As a prominent source of wireless communication, antennas have also exploited flexible substrates to realize printed antenna designs. Paper-based substrates were investigated for printed dipole and monopole antennas. Various textile-based substrates were reported for the design of patch antennas at 900 MHz and Wi-Fi frequencies [10]. Various polymer-based substrates, including liquid crystal polymer (LCP), polyimide (PI), polyethylene terephthalate (PET), polyvinylidene fluoride (PVDF), polytetrafluoroethylene (PTFE), and polydimethylsiloxane (PDMS), were reported to operate across different frequency bands. All these substrates possess different dielectric and mechanical properties that affect the antenna design characteristics [11–17].

Apart from the distinct deformation capability of polymers, such as bending, twisting, folding, and rolling, it is most desirable if they possess stretchable features. Such polymers are called elastomers. Due to their elastic nature, rubbers are often called elastomers [18, 19]. PDMS, commercially known as silicone rubber (SR), is an example of an elastomer. The relative permittivity (ε_r) of SR ranges from 2.2 to 2.9, with a dielectric loss ($\tan\delta$) of the order of 10^{-2} or less, making it suitable as a flexible substrate. Many metal patch antennas based on SR as a substrate for various frequency bands and applications have been reported. The dielectric constant of SR can be increased by adding high-dielectric constant ceramic materials, while retaining its flexural properties. Silicone rubber-ceramic composite substrates for flexible antennas have been investigated [20–22]. Likewise, other elastomeric substrates, natural rubber, butyl rubber (BR), and cyclic olefin copolymer (COC), have also found their usefulness [23, 24]. Hence, the availability of polymer and polymer-ceramic substrates has enabled the realization of flexible and conformal antennas (FCA).

The increased conducting losses in metal antennas make them inefficient for high-frequency applications. Due to the absence of inherent conductor losses, different shapes, small size, and lightweight, ease of excitation, higher modes of excitation, radiation through the whole surface, wider bandwidth, and high radiation efficiency, the dielectric resonator antennas (DRAs) are found to be the most suitable alternative in terms of performance over metal antennas [25–27]. The conventional dielectric resonator antennas reported used ceramic materials [28, 29]. Some investigations involved mounting the DRAs on rigid, non-deformable structures. Predefined curved-geometry-based DRAs were also reported, but their brittle nature limits their adaptability to arbitrary surfaces, making them unsuitable for flexible applications [30–33]. However, by proper tuning of the dielectric properties of low-loss polymer-ceramic composites, flexible DRAs can be realized. A semi-flexible DRA based on a PDMS-MCT composite resonator, developed using lithographic techniques and integrated on a non-flexible substrate for millimeter-wave applications, was investigated [34]. Although a non-metallic, flexible dielectric resonator antenna based on a ceramic-reinforced PDMS composite has been reported, its conformal analysis was not conducted [35].

The present investigation extends our earlier work [36], which reported the design and prototype realization of a flexible and conformal cylindrical dielectric resonator antenna (FC-CDRA) and its preliminary validation under cylindrical bending conditions. The proposed antenna utilizes a liquid silicone rubber-strontium titanate (LSR-ST) composite resonator integrated onto a thin LSR substrate. The dielectric and mechanical characterization of the materials, as demonstrated in our previous study [37], confirmed their suitability for flexible, conformal microwave (X-band) applications.

In this work, a thorough, systematic conformal analysis of the proposed antenna is illustrated on various non-planar geometries, including cylindrical and conical surfaces. The impact of curvature on key antenna parameters, such as resonant frequency, return loss, antenna gain, radiation efficiency, and radiation patterns is rigorously investigated and compared with the planar configuration.

Furthermore, the study establishes a comprehensive material-to-system-level framework for the proposed flexible CDRA, thereby enabling the assessment of its electromechanical behavior and bridging the gap between material characterization and practical realization. In addition, specific absorption rate (SAR) analysis is incorporated to evaluate its suitability for wearable and on-body applications.

The pivotal contributions of this research are outlined as follows, highlighting the novelty of the present work:

- Development and characterization of a flexible elastomer-ceramic (LSR-ST) composite for X-band applications
- Realization of a compact flexible CDRA (overall thickness < 2 mm) with simulation and measurement validation
- Systematic curvature analysis of the flexible CDRA under planar, cylindrical, and conical configurations

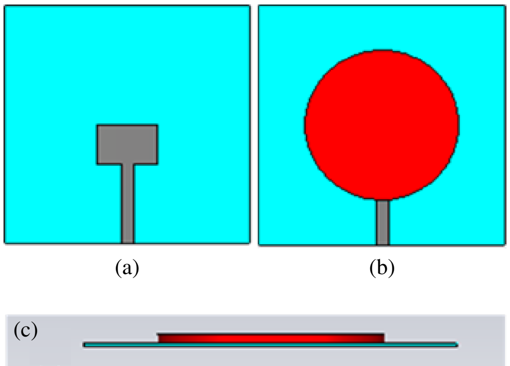

FIGURE 1. (a) Top view of the stepped-shape feedline, (b) top and (c) side views of the proposed FC-CDRA.

- Quantification of curvature-induced performance variations on antenna properties
- Demonstration of the material-dominated to geometry-dominated behavior of the antenna
- SAR evaluation for wearable and on-body applications in compliance with the international safety standards

2. MATERIAL CHARACTERIZATION

For developing the antenna prototype, materials such as liquid silicone rubber (LSR) and strontium titanate (ST) nanopowder were procured and investigated for antenna application compatibility. The LSR (pure) and LSR-ST composite (for maximum filler ratio) samples were cured and fabricated to study their electrical (ε_r and $\tan\delta$), mechanical (elongation at break), and thermal characterization, as reported in our previous studies [37]. The dielectric properties were measured using an X-band waveguide test bench setup. The results indicate stable dielectric properties with low loss, making them suitable for flexible dielectric resonator antenna applications. Dog-bone-shaped (dumbbell-shaped) samples were prepared according to ASTM D412 to measure the tensile strength (stress-strain curves) of the materials using a universal testing machine (UTM) under varying loads. The measured percentage elongation ($\%E$) as a function of applied stress reflects the elastomeric behavior of the materials essential to antenna deformation. Table 1 summarizes the measured electrical properties and the mechanical properties of the substrate and resonator.

TABLE 1. Measured dielectric and mechanical properties of materials [37].

Material	Dielectric characterization	Mechanical characterization
LSR substrate	$\varepsilon_r = 3$ $\tan\delta = 0.027$	$\%E = 550$ at 4.8 MPa
LSR-ST resonator	$\varepsilon_r = 4.25$ $\tan\delta = 0.02$	$\%E = 277$ at 3.0 MPa

*MPa — Mega Pascals

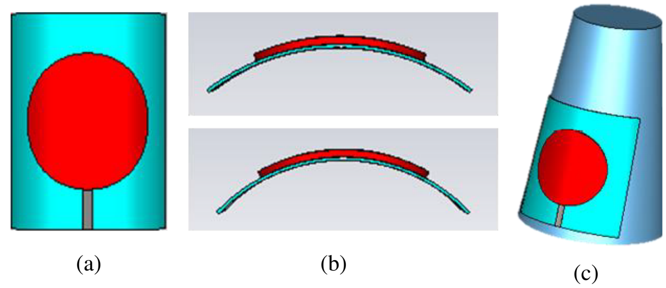

FIGURE 2. Conformal bending configurations of the proposed FC-CDRA: (a), (b) cylindrical bending (front and side views), and (c) conical bending.

3. ANTENNA DESIGN

This study investigates a flexible, conformal, cylindrical, dielectric resonator antenna (FC-CDRA) for X-band applications by exploiting salient features of a flexible LSR-ST ceramic composite. Figure 1 depicts the schematic top and side views of the LSR-ST ceramic composite-based FC-CDRA, which consists of a liquid silicone rubber-strontium titanate (LSR-ST) composite resonator with height 1 mm integrated over a 0.5 mm-thick flexible LSR substrate. The cylindrical resonator has been optimized to an aspect ratio (a/H) of 15 with radius (a) 15 mm, to ensure that the proposed antenna resonates in X-band (close to 10 GHz) and is excited by a non-resonant 50 Ω extended-stepped microstrip feedline [38–40]. The proposed antenna is $48 \times 48\,\text{mm}^2$ in size, with an overall thickness of approximately 1.6 mm. The planar and conformal configurations of the proposed antenna were simulated and analyzed in the Computer Simulation Technology (CST) simulator. The simulation results served as the basis for the prototype, which has been realized by integrating various layers using an electrically conductive silane coupling adhesive. For conformal antenna measurements, cylindrical and conical wooden fixtures with 30 mm and 40 mm radii, respectively, were used to mount the FC-CDRA. Figure 2 shows the simulated views of the FC-CDRA under cylindrical and conical bending.

4. RESULTS AND DISCUSSION

This section discusses the results of conformal antenna configuration analyses and compares them with those of a flexible planar antenna (FC-CDRA). The discussion begins with antenna design and simulation, measurements, results comparison, and validation in the planar configuration. Further, a multi-curvature bending analysis is performed to systematically assess the antenna's conformal performance over cylindrical and conical surfaces. The effect of curvature on antenna properties was analyzed and compared with measured planar and non-planar antenna performance. Additionally, the SAR analysis evaluates the proposed antenna's compliance with international safety standards.

4.1. Antenna Simulation and Measurement

The planar flexible antenna resonates at 10.076 GHz (simulated), with a return loss (S_{11}) of about -36 dB and a bandwidth of 400 MHz (VSWR < 2). The optimized feed dimen-

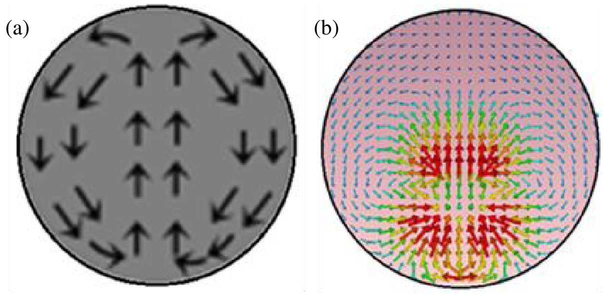

FIGURE 3. Ideal and simulated $HE_{12\delta}$ (like) mode.

sions demonstrate a non-resonant behavior of the feed at the antenna's resonant frequency. The observed excited mode within the flexible CDR was the $HE_{12\delta}$ (like) mode, as illustrated in Figure 3 and compared with the ideal field distribution [41–43].

The simulated resonant frequency of the planar antenna closely matches the analytical frequency of 9.73 GHz for the $HE_{12\delta}$ mode, as evaluated using the equation reported in prior research [36]. For the antenna prototype, the measured resonant frequency was 10.5 GHz, with a return loss of approximately -20 dB and a bandwidth (BW) of 420 MHz (VSWR < 2). Figure 4 compares the simulated and measured return losses (S_{11}) for the planar FC-CDRA.

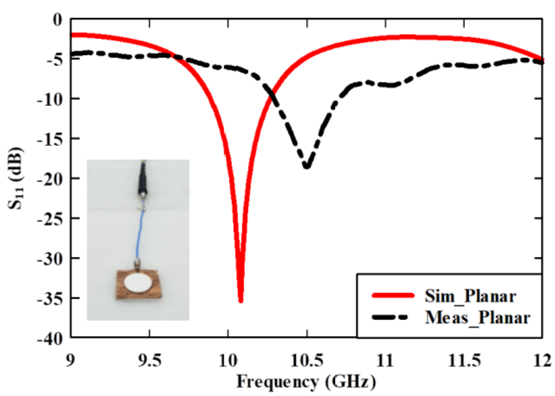

FIGURE 4. Simulated and measured S_{11} comparison of planar FC-CDRA.

Figure 5 illustrates the simulated and measured antenna gain plots (2D) of the proposed FC-CDRA in planar configuration. The antenna exhibits a simulated peak gain of 6.24 dBi at 10.076 GHz and a measured gain of 5.2 dBi at 10.5 GHz. The radiation efficiency is evaluated using the relation between gain and directivity as $G = \eta \times D$. Based on the simulated gain and directivity ($\sim$7.8 dBi), the evaluated efficiency (η) is $\sim$70%. The measured efficiency is $\sim$55% based on the measured antenna gain and estimated directivity, as evidenced by the stable radiation patterns.

The proposed antenna radiates in the broadside direction with linear polarization. Figure 6 compares polar radiation patterns in the E- and H-planes.

Figures 7(a) and (b) illustrate the simulated and measured normalized radiation patterns (co-pol and x-pol) in the E- and H-planes. Both planes exhibit a stable co-polarized radiation pattern with approximately 1–2 dB peak variation. The mea-

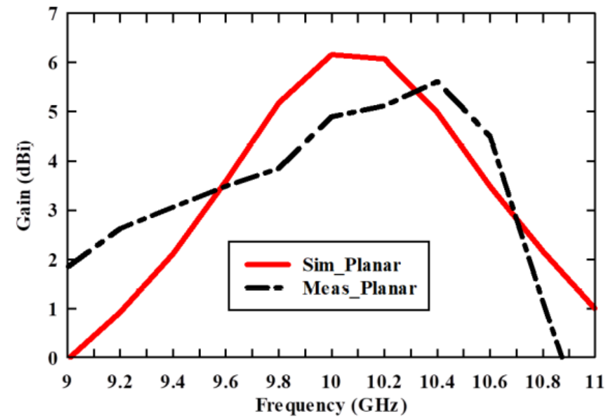

FIGURE 5. Simulated and measured gain comparison of planar FC-CDRA.

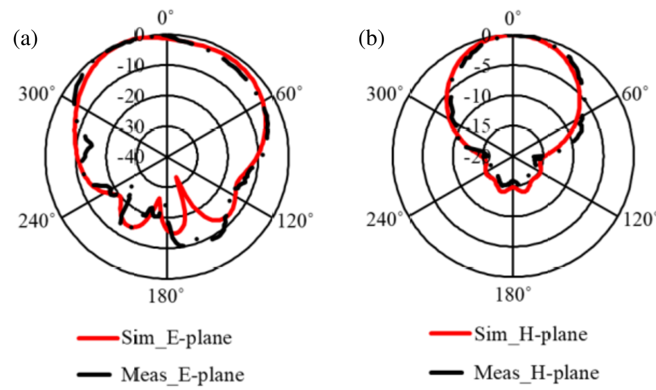

FIGURE 6. Simulated and measured radiation patterns of planar FC-CDRA. (a) E-plane and (b) H-plane.

sured pattern shows slight asymmetry and noticeable ripples in the E-plane. In contrast, the simulated pattern shows none, suggesting that these features may be attributable to fabrication tolerances and the measurement setup.

On the other hand, the H-plane demonstrates a symmetrical co-polarized pattern. Further, the measured cross-polarization level in both planes increases relative to the simulated results due to measurement uncertainties, as expected, yet remains typically suppressed below -20 dB. Thus, close agreement between simulated and measured co- and cross-polarization results in both the E-plane and H-plane confirms the validity of the proposed antenna.

4.2. Deviation in Antenna Parameters

The simulated and measured results show deviations in resonant frequency, return loss (S_{11}), bandwidth, gain, and radiation pattern of the proposed flexible antenna. The resonant frequency of a CDRA is primarily dependent on its effective dielectric constant and geometrical dimensions, as expressed in the following relation, $f_r \propto 1/a\sqrt{\varepsilon_r}$ where 'a' is the radius of the resonator and ε_r is the dielectric constant. This relationship indicates that even small variations of about 0.2–0.3 in material properties ($\Delta\varepsilon_r$) or geometrical dimensions can lead to noticeable shifts in the resonant frequency.

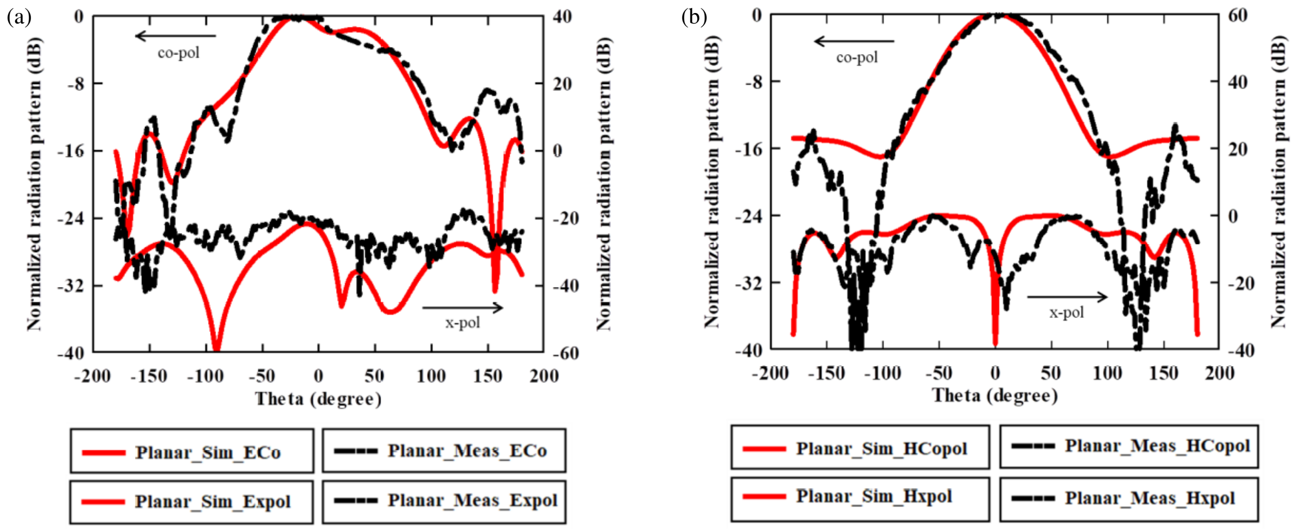

FIGURE 7. (a) Simulated and measured normalized E-plane co-pol and x-pol radiation patterns. (b) Simulated and measured normalized H-plane co-pol and x-pol radiation patterns.

A discernible $\sim$4.2% variation in measured and simulated resonant frequencies arises from several factors. They include material inhomogeneity, dielectric dispersion at high frequencies, and nonuniform filler distribution within the LSR-ST composite. A variation of about 0.2–0.3 in the effective dielectric constant causes a resonance shift of $\sim$3–5%. Furthermore, the presence of a thin silane coupling layer (thickness $\sim$20–40 µm) not modeled in the simulation slightly decreases the resonator's effective permittivity. The formation of micro air gaps during bonding accounts for an additional 1–2% upward shift in the frequency. Fabrication tolerances, such as ± 0.1 mm geometrical variations in substrate and resonator dimensions, are also attributable to a $\sim$1–2% deviation. Moreover, limitations in material modeling and the assumption of ideal dielectric behavior in simulations do not completely capture the material's dispersion and electromechanical properties. Thus, the combined effect of these factors reasonably contributes to a $\sim$4.2% frequency shift.

The measured loss tangent of the resonator material, misalignment of the feed, variations in the input impedance due to feed dimensions and substrate thickness, and minor material variations reduce return loss magnitude. The lower Q value due to material and interfacial losses, as well as the coupling layer, results in a bandwidth deviation. Dielectric losses (tangent loss ($\tan\delta$)), inherent microstructural effects, fabrication tolerances, calibration-related losses, and scattering losses degrade radiation efficiency and, in turn, antenna gain. The discrepancies in the results are realistic and accepted, validating the proposed flexible antenna functionality.

4.3. Bending Analyses

The bending analyses of the flexible CDRA presented in this section were carried out by wrapping or mounting the antenna over non-planar surfaces, followed by testing and measurement. For simulation, conformal antenna configurations were modeled using vacuum-filled cylindrical and conical surfaces, thereby neglecting any material loading effects. In contrast, to provide mechanical support, wooden fixtures have been deployed to obtain real-time measurements of the FC-CDRA prototype antenna.

The bending of a flexible CDRA over non-planar curved surfaces induces variations in input impedance, return loss, resonant frequency, field distribution, gain, radiation efficiency, and radiation pattern. However, the antenna deformation on these curved surfaces inhibits the curvature effect [44–49].

4.3.1. Effect of Curvature on Resonant Frequency and Radiation Characteristics

The conformal performance of the proposed antenna under cylindrical and conical bending conditions can be well explained by electromagnetic (EM) theory, considering combined effects of the effective electrical length (L_{eff}) and effective permittivity (ε_{eff}), as well as geometry-induced field redistribution. The antenna's resonant frequency obeys the relation, $f_r \propto 1/(L_{eff}\sqrt{\varepsilon_{eff}})$ indicating that the effective electrical length and permittivity govern the shift in the resonant frequency. The radiation pattern and gain showed degradation with increasing curvatures and distinct geometrical surfaces.

(1) Cylindrical Bending Analysis

The antenna's simulated resonant frequencies under cylindrical bending with increasing curvature (radii from 40 mm to 30 mm) showed a downward frequency shift comparable to that of a planar antenna. The antenna exhibits uniformity along the curvature attributed to symmetrical strain distribution, resulting in partial cancellation of permittivity variations. Due to material-dependent behavior, the frequency response is predominantly affected. Further, the electromechanical interactions within the flexible substrate and resonator are neglected in the simulation analysis, leading to a downward frequency shift due to enhanced dielectric loading from curvature. However, the measurements show an upward frequency shift similar to

TABLE 2. Comparison of antenna parameters for planar and cylindrical bend FC-CDRA.

Parameters	Planar FC-CDRA	Cylindrical bend FC-CDRA	
		$r = 40$ mm	$r = 30$ mm
Frequency (GHz)	10.076	10.62	10.7
Realized Gain (dBi)	5.2	4.24	3.98
Radiation Efficiency (%η)	∼55	∼44	∼40

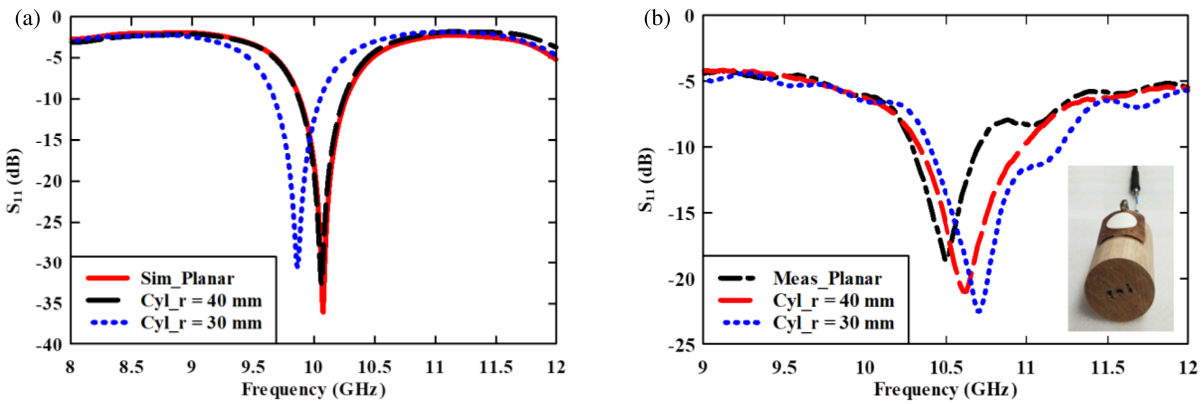

FIGURE 8. (a) Simulated S_{11} comparison of planar and cylindrical bend FC-CDRA. (b) Measured S_{11} comparison of planar and cylindrical bend FC-CDRA.

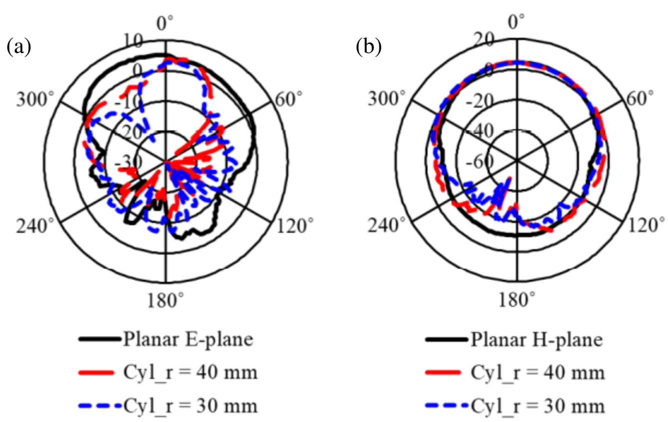

FIGURE 9. Measured radiation pattern of planar and cylindrical bend FC-CDRA. (a) E-plane and (b) H-plane.

that observed in the planar configuration, consistent with conformal antenna theory.

Figures 8(a) and (b) elucidate the simulated and measured S_{11} for 40 mm and 30 mm bending radii and compare them with those of the planar flexible CDRA. Due to impedance mismatch and stretching of the elastomeric substrate and resonator, the return loss magnitude increased slightly. The resonant frequencies for cylindrical bending of the antenna are 10.62 GHz (-21 dB) and 10.7 GHz (-22.5 dB), with bandwidths of 640 MHz and 800 MHz for varying curvatures. The combined effects of effective permittivity variation and impedance matching under deformation primarily determine the antenna bandwidth, rather than permittivity alone.

The measured gain decreased gradually with increasing curvature (radii from 40 mm to 30 mm). The E-plane maintains a broadside radiation pattern, with significant distortion and varying side-lobe levels, thus indicating increasing structural deformation. On the other hand, the H-plane demonstrated a relatively stable omnidirectional (like) pattern closely matching the planar antenna radiation pattern, thereby confirming its robustness against mechanical deformation. Table 2 summarizes and compares the antenna resonance, gain, and estimated radiation efficiency for various cylindrical bending radii relative to the planar configuration.

The simulated normalized radiation patterns observed are in close agreement with the measured results. The E-plane and H-plane co-pol pattern shows a 1–2 dB deviation, and the x-pol levels remain below -20 dB, highlighting polarization purity and low sensitivity to deformation. Figure 9 shows the measured gain pattern (polar), and Figures 10(a) and (b) depict the cylindrical configurations (bending radii of 40 mm and 30 mm) with the proposed planar antenna in the E-plane and H-plane.

(2) Conical Bending Analysis

The flexible antenna prototype was wrapped around a conical surface (frustum of a cone) with bottom radii (r_b) of 40 mm and 30 mm, top radii (r_t) of 20 mm and ∼17 mm, and heights (h) of ∼70 mm and ∼85 mm. The effective local radius (r_c) at the antenna center location on the conical surface has been calculated using Equation (1) to be 30 mm and ∼23.5 mm, respectively. The nonuniform curvature introduced by conical bending [57–59] results in spatial deviations in both strain and electromagnetic field distributions. Spatial variation in effective permittivity or geometry redistributes the electromagnetic field. The tapering of the geometrical surface results in greater field concentration at the smaller radius (the top radius), thereby

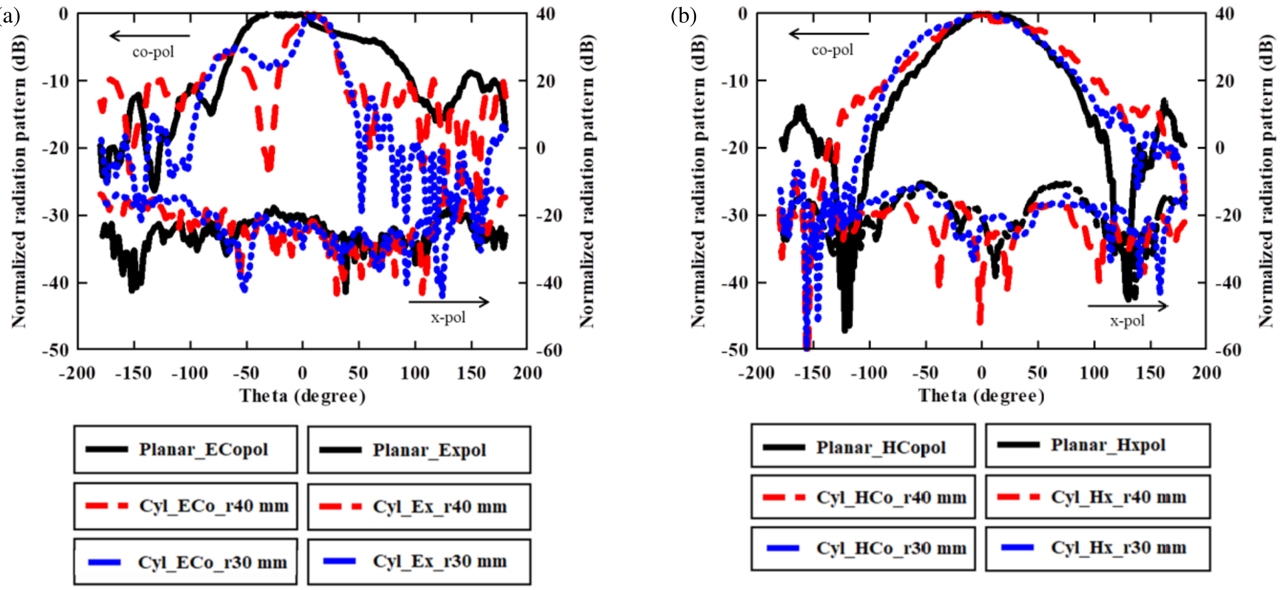

FIGURE 10. (a) Measured normalized E-plane co-pol and x-pol radiation patterns of planar and cylindrical bend FC-CDRA. (b) Measured normalized H-plane co-pol and x-pol radiation patterns of planar and cylindrical bend FC-CDRA.

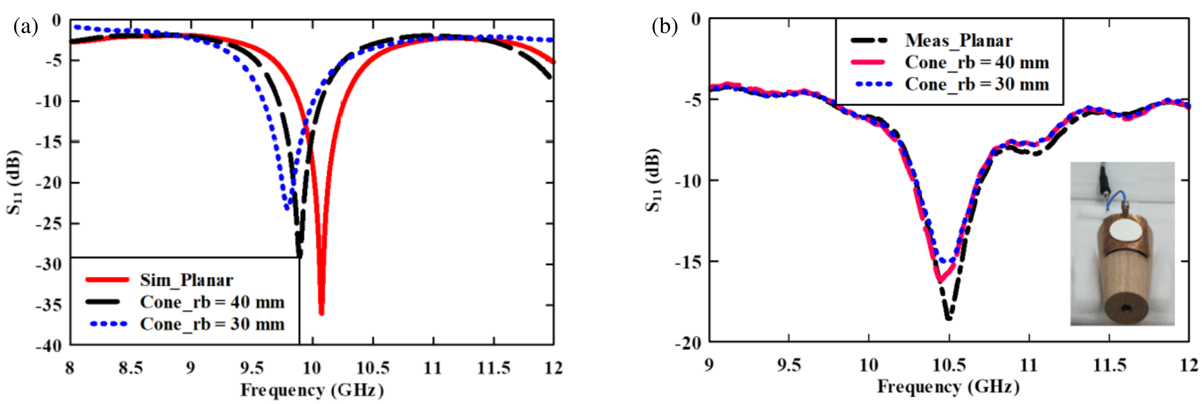

FIGURE 11. (a) Simulated S_{11} comparison of planar and conical bend FC-CDRA. (b) Measured S_{11} comparison of planar and conical bend FC-CDRA.

increasing electromagnetic energy confinement within the dielectric. In addition, the compressive strain in these tapering regions increases permittivity, thereby dominating the effective electrical length variation and leading to a downward frequency shift in both simulations and measurements, thus exhibiting the strain-dependent permittivity behavior of the elastomer-based materials.

$$r_c = r_b - \frac{(r_b - r_t)}{h}(z_c) \tag{1}$$

where z_c is the axial distance from the base.

According to dielectric resonator antenna (DRA) theory, this phenomenon is consistent with the idea that increased field confinement in the dielectric medium results in a downward frequency shift. Figures 11(a) and (b) compare the simulated and measured S_{11} for the conformal, flexible CDRA on various conical curvatures with the planar antenna. The return loss magnitude slightly increases due to impedance mismatch and stretching of the elastomeric substrate and resonator. The resonances under conical deformation are 10.48 GHz (-15.2 dB) and 10.44 GHz (-16 dB), with bandwidths of 410 MHz and 380 MHz for 40 mm and 30 mm, respectively.

The radiation pattern in the E-plane shows a noticeable distortion due to the antenna's conical bending compared to a planar antenna. The main lobe appears more asymmetric with increased ripples and side lobes for a radius (r_b) of 40 mm. As the curvature increases (from 40 mm to 30 mm), the distortion increases further, indicating nonuniform strain and perturbations in the current due to conical geometry (tapering surface), which also result in higher side-lobe levels that alter the radiation distribution. The peak gain reduces to 2–3 dB as curvature increases. At the same time, a relatively stable, omnidirectional (like) pattern was observed for varying curvatures, confirming the H-plane's low sensitivity to deformation. The observed gain variation in the H-plane is minimal, with slightly increasing ripples. Figure 12 illustrates gain patterns (polar) in the E- and H-planes for conical bending. Table 3 summarizes

TABLE 3. Comparison of antenna parameters for planar and conical bend FC-CDRA.

Parameters	Planar FC-CDRA	Conical bend FC-CDRA	
		$r_b = 40$ mm	$r_b = 30$ mm
Frequency (GHz)	10.076	10.48	10.44
Realized Gain (dBi)	5.2	3.77	3.24
Radiation efficiency ($\%\eta$)	∼55	∼40	∼35

*r_b — base radius

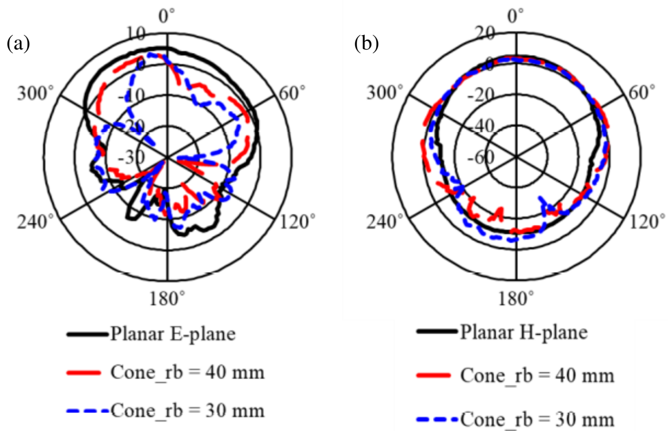

FIGURE 12. Measured radiation pattern of planar and conical bend FC-CDRA. (a) E-plane and (b) H-plane.

and compares the antenna resonance, gain, and estimated radiation efficiency for various conical bending radii relative to the planar configuration.

Figures 13(a) and (b) show the normalized E-plane and H-plane (co-pol and x-pol) patterns for conical deformation. The E-plane co-polarized pattern retains broadside radiation with significant distortions compared to the planar co-polar pattern. The H-plane maintains a stable, almost omnidirectional co-polarized pattern, while the corresponding cross-polarization levels in E-plane rise to -15 dB and remain comparatively well suppressed below -20 dB in H-plane due to a symmetric pattern.

The bending analysis indicates that the antenna's cylindrical bending has a lesser impact on the radiation characteristics, highlighting the importance of curvature uniformity and reliability of the proposed flexible antenna for conformal applications. The observed variations in resonant frequency and impedance characteristics under deformation can thus be attributed to both geometric and material effects, as the flexible dielectric materials undergo strain-induced changes in permittivity and may exhibit anisotropic behavior. Further, surface curvature alters the current distribution and effective electrical length, thereby influencing the overall electromagnetic performance as explained by conformal antenna theory [60].

4.4. SAR Analysis

The conformal analysis of the proposed antenna, discussed in the preceding sections, demonstrates the electromagnetic performance under deformation on various non-planar surfaces. To evaluate the antenna's suitability for on-body applications, it is essential to assess the electromagnetic energy absorption by human tissue. Therefore, to ensure compliance with international safety standards, a specific absorption rate (SAR) analysis was performed.

TABLE 4. Properties and thicknesses of various tissue layers of the human arm model at X-band.

Layer	Relative Permittivity (ε_r)	Conductivity (σ) S/m	Thickness (mm)
Skin	41	9	2
Fat	5.3	0.5	3
Muscle	49	10.5	15
Bone	12	2	8

For SAR analysis, a realistic anatomical multilayer human tissue model, comprising skin, fat, muscle, and bone, was employed. The antenna was directly mounted on the skin layer to illustrate its practical use. The relative permittivity (ε_r) and conductivity (σ) of human tissues were adopted from a widely accepted database [61]. At the same time, the standard values were used for mass density (ρ) of the various layers of the model. Using the CST simulator, the SAR computation for 10 g and 1 g mass averaging at the 10.168 GHz antenna resonant frequency, with a normalized input power of 1 W, was performed according to the IEEE/IEC 62704-1 standard [62]. Table 4 summarizes the properties and thicknesses of the various tissue layers for the human arm model simulation at X-band.

Equation (2) determines the distribution of SAR within the tissue.

$$\text{SAR} = \frac{\sigma|E|^2}{\rho}\ (\text{W/kg}) \tag{2}$$

where, σ — Electrical conductivity of the tissue (S/m), $|E|$ — Electric field magnitude (V/m), ρ — Mass density (kg/m^3).

The peak SAR value for the 10 g averaged mass was 1.26 W/kg, which falls well below the 2 W/kg limit for general public exposure specified by the International Commission on Non-Ionizing Radiation Protection (ICNIRP) safety guidelines [63]. Thus, the results confirm the proposed antenna's suitability for on-body applications and its good electromagnetic confinement.

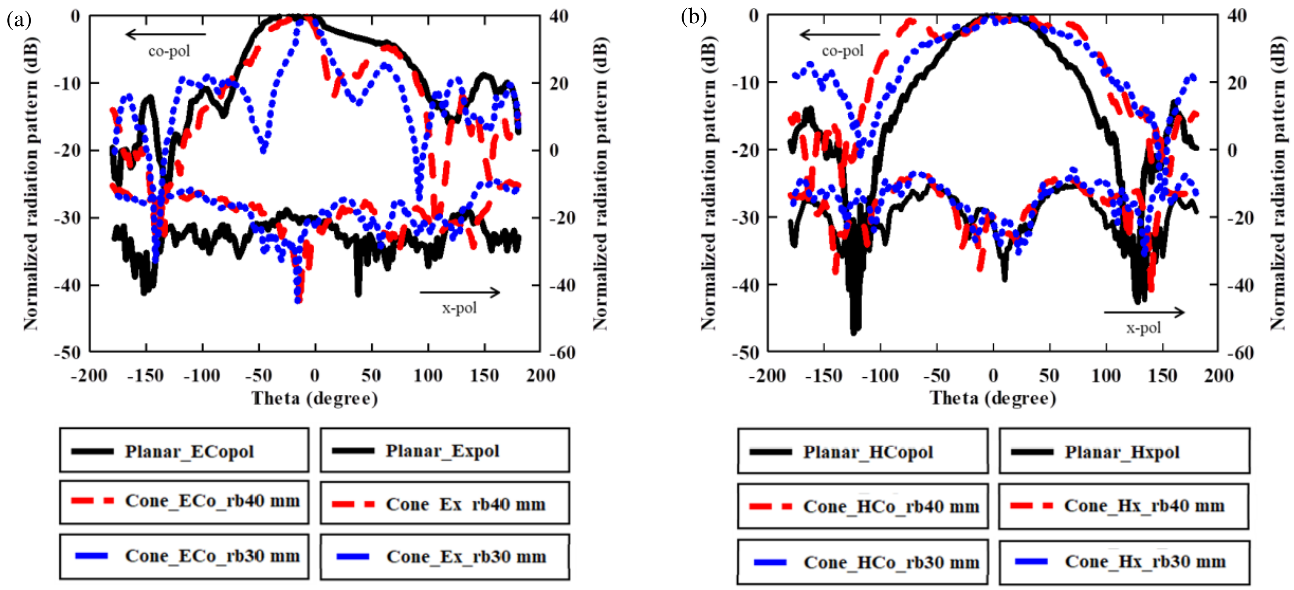

FIGURE 13. (a) Measured normalized E-plane co-pol and x-pol radiation patterns of planar and conical bend FC-CDRA. (b) Measured normalized H-plane co-pol and x-pol radiation patterns of planar and conical bend FC-CDRA.

TABLE 5. Comparison of proposed FC-CDRA with the reported DRAs.

Parameters	[30]	[31]	[34]	[35]	[52]	**Proposed**
Dielectric resonator	Taconic RF-10	Alumina	PDMS-MCT	PDMS-Ceramic	Roger RT 6010	**LSR-ST**
Substrate	-	FR-4	Taconic TLY-5	PDMS	Roger RT 5880	**LSR**
Antenna size (mm^2)	20	33×20	35×35	40×40	$\sim$79	**48×48**
Feeding technique	Coaxial feed	Slot-coupled	Slot-coupled	Carbon microstrip feed	Slot-coupled	**Stepped microstrip feed**
f_r (GHz)	$\sim$8	$\sim$7.6	$\sim$26	5.8	$\sim$60	**10.5**
Excited mode	TM	$TM^z_{11\delta}$	TE	$HE_{11\delta}$	$EH_{11\delta}$	**$HE_{12\delta}$**
Bandwidth (BW)	7.23–9.82	6.9–8.3	21–29	5.8–9.4	59–62	**10.27–10.72 (planar)**
Gain (dBi)	9.6	$\sim$7	4.9	N/A	$\sim$5 (simulated)	**5.2 (planar)**
Radiation efficiency (% η)	93	N/A	N/A	N/A	$\sim$97 (simulated)	**$\sim$55 (planar)**
Flexible/Conformal	Conformal	Conformal	Partially flexible	Flexible	Conformal	**Flexible & Conformal**
Conformal bending analysis	Yes	No	No	No	Yes	**Yes**
Bending radius (r) mm	60	17 (fixed)	-	-	10	**40 mm 30 mm**
Specific Absorption Rate (SAR)	No	No	No	No	No	**Yes 1.26 W/kg**

In contrast, the 1 g peak SAR value was 9.06 W/kg at the operating frequency, exceeding the 1.6 W/kg limit defined by IEEE C95.1 for general public exposure [64]. This higher peak in SAR is attributable to strong localized surface absorption at the antenna-skin layer interface due to shallow (reduced) penetration depth at 10 GHz. The depth of penetration (δ) varies inversely proportional to the square root of the frequency, as defined in Equation (3). The 1 g averaged mass SAR illustrates

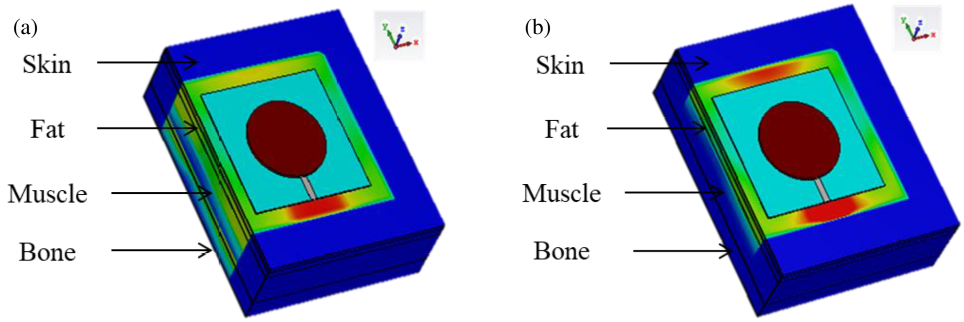

FIGURE 14. (a) SAR analysis (sub volume) of human arm tissue model for 10 g averaged mass. (b) SAR analysis (sub volume) of human arm tissue model for 1 g averaged mass.

highly localized absorption owing to its small averaging volume. In contrast, the 10 g SAR, averaged over a larger volume extending beyond the skin layer (the effective penetration depth), yields a lower SAR value. Figures 14(a) and (b) elucidate (cross-sectional view) the SAR evaluation in the simulator for 10 g and 1 g averaged mass.

$$\delta \propto \frac{1}{\sqrt{f}} \tag{3}$$

The evaluated differences between 1 g and 10 g peak SAR values at the same frequency arise from the combined effects of frequency-dependent (electromagnetic) penetration depth and spatial mass averaging across various tissue layers. However, this SAR performance is consistent with the bio-electromagnetic theory and the SAR evaluation standards (IEEE/IEC 62704-1).

4.5. Comparison

To date, several rigid conformal DRAs have been reported based on ceramic and polymer-composite materials. Very few studies report on flexible polymer-composite-based DRAs. Table 5 summarizes and compares the proposed flexible DRA design with the existing literature. Parameters such as DRA material and substrate, antenna size, feeding technique, resonating frequency, excited mode, bandwidth, gain, radiation efficiency, flexibility, conformability, curvature analysis, bending radii, and SAR evaluation were compared.

5. CONCLUSION

A conformal analysis of a flexible cylindrical dielectric resonator antenna (FC-CDRA) subjected to various deformations over non-planar surfaces has been presented in this study. The effect of curvature on key antenna parameters, including resonant frequency, return loss, impedance bandwidth, gain, and radiation characteristics, was systematically examined. The resonant frequencies for cylindrical bending of the antenna are 10.62 GHz (-21 dB) and 10.7 GHz (-22.5 dB) for 40 mm and 30 mm radii, respectively. In contrast, the resonances under conical deformation are 10.48 GHz (-15.2 dB) and 10.44 GHz (-16 dB). The antenna's resonance performance under cylindrical bending highlighted the material-dominated behavior. In contrast, conical bending demonstrated a geometry-dominated response, validating the robustness and reliability of the proposed FC-CDRA. For bending radii of 40 mm and 30 mm, the measured bandwidths are 640 MHz and 800 MHz for cylindrical bending, while for conical bending, the measured bandwidths are 410 MHz and 380 MHz, respectively. The antenna's bandwidth under deformation was determined by the combined effects of effective permittivity, impedance matching, geometry, and current redistribution due to curvature. Due to nonuniform curvatures and associated field perturbations, in the case of conical bending, there is a significant degradation of radiation properties compared to cylindrical bending, primarily due to nonuniform curvatures and associated field perturbations. The computed peak SAR values indicate compliance with public safety exposure limits for a 10 g averaged mass of human tissue. Therefore, the study concludes that the proposed antenna exhibited stable performance for planar, cylindrical, and conical bending configurations, supporting its suitability for X-band applications. They include wearable antennas, on-body sensing and short-range high-frequency communication systems, UAV-based surveillance systems, airborne conformal antennas, and satellite communication operating in the 10.26–11.2 GHz frequency band.

REFERENCES

[1] Josefsson, L. and P. Persson, *Conformal Array Antenna Theory and Design*, Wiley, 2006.

[2] Wong, K.-L., *Design of Nonplanar Microstrip Antennas and Transmission Lines*, John Wiley & Sons, 2001.

[3] Anjum, A. and J. C. Mudiganti, "Effect of curvature on a X-band conformal microstrip patch antenna," in *2019 IEEE Indian Conference on Antennas and Propogation (InCAP)*, 1–3, Ahmedabad, India, 2019.

[4] Thomas, W., R. C. Hall, and D. I. Wu, "Effects of curvature on the fabrication of wraparound antennas," in *IEEE Antennas and Propagation Society International Symposium. 1997 Digest*, Vol. 3, 1512–1515, Montreal, QC, Canada, 1997.

[5] Elrashidi, A., K. Elleithy, and H. Bajwa, "The fringing field and resonance frequency of cylindrical microstrip printed antenna as a function of curvature," *International Journal of Wireless Communications and Networking (IJWCN)*, 2011.

[6] Mahros, A. M., M. M. Tharwat, and A. Elrashidi, "A novel performance analysis of the microstrip antenna printed on a cylindrical body," *International Journal of Antennas and Propagation*,

Vol. 2014, No. 1, 613245, 2014.
[7] Khaleel, H., *Innovation in Wearable and Flexible Antennas*, WIT Press, 2015.
[8] Paracha, K. N., S. K. A. Rahim, P. J. Soh, and M. Khalily, "Wearable antennas: A review of materials, structures, and innovative features for autonomous communication and sensing," *IEEE Access*, Vol. 7, 56 694–56 712, 2019.
[9] Kirtania, S. G., A. W. Elger, M. R. Hasan, A. Wisniewska, K. Sekhar, T. Karacolak, and P. K. Sekhar, "Flexible antennas: A review," *Micromachines*, Vol. 11, No. 9, 847, 2020.
[10] Ahmed, M. I., M. F. Ahmed, and A. A. Shaalan, "Novel electrotextile patch antenna on jeans substrate for wearable applications," *Progress In Electromagnetics Research C*, Vol. 83, 255–265, 2018.
[11] Riheen, M. A., T. Nguyen, T. K. Saha, T. Karacolak, and P. K. Sekhar, "CPW fed wideband bowtie slot antenna on PET substrate," *Progress In Electromagnetics Research C*, Vol. 101, 147–158, 2020.
[12] Ahmed, S., F. A. Tahir, A. Shamim, and H. M. Cheema, "A compact Kapton-based inkjet-printed multiband antenna for flexible wireless devices," *IEEE Antennas and Wireless Propagation Letters*, Vol. 14, 1802–1805, 2015.
[13] Bai, X., W.-Y. Han, and L.-J. Xu, "Multi-band energy harvesting antenna based on PVDF piezoelectric material," in *2019 International Applied Computational Electromagnetics Society Symposium — China (ACES)*, 1–2, Nanjing, China, 2019.
[14] Lin, C.-P., C.-H. Chang, Y.-T. Cheng, and C. F. Jou, "Development of a flexible SU-8/PDMS-based antenna," *IEEE Antennas and Wireless Propagation Letters*, Vol. 10, 1108–1111, 2011.
[15] Simorangkir, R. B. V. B., Y. Yang, K. P. Esselle, and B. A. Zeb, "A method to realize robust flexible electronically tunable antennas using polymer-embedded conductive fabric," *IEEE Transactions on Antennas and Propagation*, Vol. 66, No. 1, 50–58, 2018.
[16] Salleh, S. M., M. F. Ain, Z. Ahmad, I. S. Z. Abidin, L. Y. Seng, and M. N. Osman, "Stretchable and bendable polydimethylsiloxane-silver composite antenna on PDMS/air gap substrate for 5G wearable applications," *IEEE Access*, Vol. 11, 133 623–133 639, 2023.
[17] Du, C., X. Li, and S. Zhong, "Compact liquid crystal polymer based tri-band flexible antenna for WLAN/WiMAX/5G applications," *IEEE Access*, Vol. 13, 123 259–123 268, 2019.
[18] Sharma, P. K., N. Gupta, and P. I. Dankov, "Characterization of polydimethylsiloxane (PDMS) as a wearable antenna substrate using resonance and planar structure methods," *AEU — International Journal of Electronics and Communications*, Vol. 127, 153455, 2020.
[19] Awang, Z., N. A. M. Affendi, N. A. L. Alias, and N. A. M. Razali, "Flexible antennas based on natural rubber," *Progress In Electromagnetics Research C*, Vol. 61, 75–90, 2016.
[20] Babar, A. A., V. A. Bhagavati, L. Ukkonen, A. Z. Elsherbeni, P. Kallio, and L. Sydänheimo, "Performance of high-permittivity ceramic-polymer composite as a substrate for UHF RFID tag antennas," *International Journal of Antennas and Propagation*, Vol. 2012, No. 1, 905409, 2012.
[21] Koulouridis, S., G. Kiziltas, Y. Zhou, D. J. Hansford, and J. L. Volakis, "Polymer-ceramic composites for microwave applications: Fabrication and performance assessment," *IEEE Transactions on Microwave Theory and Techniques*, Vol. 54, No. 12, 4202–4208, 2006.
[22] Zhang, R., J. Liu, Y. Wang, Z. Luo, B. Zhang, and J. Duan, "Flexible wearable composite antennas for global wireless communication systems," *Sensors*, Vol. 21, No. 18, 6083, 2021.
[23] Sebastian, M. T., R. Ubic, and H. Jantunen, *Microwave Materials and Applications*, John Wiley & Sons, 2017.
[24] Al-Sehemi, A. G., A. A. Al-Ghamdi, N. T. Dishovsky, P. Malinova, N. T. Atanasov, and G. L. Atanasova, "Natural rubber composites containing low and high dielectric constant fillers and their application as substrates for compact flexible antennas," *Polym. Polym. Compos.*, Vol. 29, 233–245, 2021.
[25] Luk, K. M. and K. W. Leung, *Dielectric Resonator Antenna*, Research Studies Press, 2003.
[26] Petosa, A. and A. Ittipiboon, "Dielectric resonator antennas: A historical review and the current state of the art," *IEEE Antennas and Propagation Magazine*, Vol. 52, No. 5, 91–116, 2010.
[27] Dash, S. K. K., T. Khan, and A. De, "Dielectric resonator antennas: An application oriented survey," *International Journal of RF and Microwave Computer-Aided Engineering*, Vol. 27, No. 3, e21069, 2017.
[28] Long, S., M. McAllister, and L. Shen, "The resonant cylindrical dielectric cavity antenna," *IEEE Transactions on Antennas and Propagation*, Vol. 31, No. 3, 406–412, 1983.
[29] Kishk, A. A., Y. Yin, and A. W. Glisson, "Conical dielectric resonator antennas for wide-band applications," *IEEE Transactions on Antennas and Propagation*, Vol. 50, No. 4, 469–474, 2002.
[30] Mishra, M., A. Rajput, P. K. Gupta, and B. Mukherjee, "A low profile perturbed CDRA with convex conformal ground plane excited by differential feed," *AEU — International Journal of Electronics and Communications*, Vol. 173, 155033, 2024.
[31] Ma, B., J. Pan, E. Wang, and Y. Luo, "Conformal bent dielectric resonator antennas with curving ground plane," *IEEE Transactions on Antennas and Propagation*, Vol. 67, No. 3, 1931–1936, 2019.
[32] Ma, B., J. Pan, E. Wang, and D. Yang, "Miniaturized conformal arc dielectric resonator antennas using dielectric and metallic loading," *IEEE Access*, Vol. 7, 139 518–139 525, 2019.
[33] Gupta, P. K., M. Mishra, G. Tiwari, and B. Mukherjee, "A low-profile DRA on convex conformal ground plane for C and X band applications," *Int. J. Electron.*, Vol. 113, No. 1, 146–160, 2026.
[34] Rashidian, A., D. M. Klymyshyn, M. T. Aligodarz, M. Boerner, and J. Mohr, "Development of polymer-based dielectric resonator antennas for millimeter-wave applications," *Progress In Electromagnetics Research C*, Vol. 13, 203–216, 2010.
[35] Chen, S. J. and C. Fumeaux, "A concept of flexible non-metallic dielectric resonator antenna for conformal applications," in *2020 14th European Conference on Antennas and Propagation (EuCAP)*, 1–4, Copenhagen, Denmark, 2020.
[36] Anjum, A. and J. C. Mudiganti, "Flexible cylindrical dielectric resonator antenna for X-band satellite, space, wireless sensor networks, and flexible applications," *IEEE Access*, Vol. 14, 3216–3228, 2026.
[37] Anjum, A. and J. C. Mudiganti, "Optimization of flexible, low-loss, and temperature-stable strontium titanate-reinforced liquid silicone rubber composite for next-generation microwave applications," *Advanced Composite Materials*, 1–22, 2026.
[38] Balanis, C. A., *Antenna Theory: Analysis and Design*, John Wiley & Sons, New York, 2010.
[39] Kranenburg, R. A. and S. A. Long, "Microstrip transmission line excitation of dielectric resonator antennas," *Electronics Letters*, Vol. 24, No. 18, 1156–1157, 1988.
[40] Rashidian, A., M. T. Aligodarz, L. Shafai, and D. M. Klymyshyn, "On the matching of microstrip-fed dielectric resonator antennas," *IEEE Transactions on Antennas and Propagation*, Vol. 61, No. 10, 5291–5296, 2013.
[41] Kajfez, D. and P. Guillon, *Dielectric Resonators*, Artech House, 1986.

[42] Guha, D., A. Banerjee, C. Kumar, and Y. M. M. Antar, "Higher order mode excitation for high-gain broadside radiation from cylindrical dielectric resonator antennas," *IEEE Transactions on Antennas and Propagation*, Vol. 60, No. 1, 71–77, 2012.

[43] Rana, B. and S. K. Parui, "Nonresonant microstrip patch-fed dielectric resonator antenna array," *IEEE Antennas and Wireless Propagation Letters*, Vol. 14, 747–750, 2015.

[44] Ali Khan, M. U., R. Raad, F. Tubbal, P. I. Theoharis, S. Liu, and J. Foroughi, "Bending analysis of polymer-based flexible antennas for wearable, general IoT applications: A review," *Polymers*, Vol. 13, No. 3, 357, 2021.

[45] Elrashidi, A., K. Elleithy, and H. Bajwa, "Input impedance, VSWR and return loss of a conformal microstrip printed antenna for TM_{01} mode using two different substrates," *International Journal of Networks and Communications*, Vol. 2, No. 2, 13–19, 2012.

[46] Erturk, V. B. and R. G. Rojas, "Efficient analysis of input impedance and mutual coupling of microstrip antennas mounted on large coated cylinders," *IEEE Transactions on Antennas and Propagation*, Vol. 51, No. 4, 739–749, 2003.

[47] Bai, Q. and R. Langley, "Crumpled textile antennas," *Electronics Letters*, Vol. 45, No. 9, 436–438, 2009.

[48] Bai, Q. and R. Langley, "Textile antenna bending and crumpling," in *Proceedings of the Fourth European Conference on Antennas and Propagation*, 1–4, Barcelona, Spain, 2010.

[49] Ashkenazy, J., S. Shtrikman, and D. Treves, "Electric surface current model for the analysis of microstrip antennas on cylindrical bodies," *IEEE Transactions on Antennas and Propagation*, Vol. 33, No. 3, 295–300, 1985.

[50] Krowne, C., "Cylindrical-rectangular microstrip antenna," *IEEE Transactions on Antennas and Propagation*, Vol. 31, No. 1, 194–199, 1983.

[51] Ali, S. M., T. M. Habashy, J.-F. Kiang, and J. A. Kong, "Resonance in cylindrical-rectangular and wraparound microstrip structures," *IEEE Transactions on Microwave Theory and Techniques*, Vol. 37, No. 11, 1773–1783, 1989.

[52] Chorfi, H., M. Nedil, Y. Coulibaly, T. A. Denidni, I. B. Mabrouk, and L. Talbi, "A dielectric resonator antenna mounted on a conformal structure at 60 GHz," in *2011 IEEE International Symposium on Antennas and Propagation (APSURSI)*, 2577–2580, Spokane, WA, USA, 2011.

[53] Chorfi, H., M. Nedil, I. B. Mabrouk, T. A. Denidni, and L. Talbi, "Design of a 60 GHz dielectric resonator antenna array mounted on a conformal structure," in *Proceedings of the 2012 IEEE International Symposium on Antennas and Propagation*, 1–2, Chicago, IL, USA, 2012.

[54] Zainud-Deen, S., H. A. E.-A. Malhat, and K. Awadalla, "Dielectric resonator antenna mounted on a circular cylindrical ground plane," *Progress In Electromagnetics Research B*, Vol. 19, 427–444, 2010.

[55] Zainud-Deen, S. H., N. A. El-Shalaby, and K. H. Awadalla, "Radiation characteristics of cylindrical dielectric resonator antenna mounted on superquadric cylindrical body," *Electrical and Electronic Engineering*, Vol. 2, No. 3, 88–95, 2012.

[56] Jilani, S. F., M. O. Munoz, Q. H. Abbasi, and A. Alomainy, "Millimeter-wave liquid crystal polymer based conformal antenna array for 5G applications," *IEEE Antennas and Wireless Propagation Letters*, Vol. 18, No. 1, 84–88, 2019.

[57] Biswas, D. and V. Ramachandra, "A novel approach to design conformal frustum wrap around antenna," in *Proceedings of the International Radar Symposium India (IRSI)*, 190–193, Bangalore, India, 2013.

[58] Shavit, R., "Circular polarization microstrip array on a conical surface," in *IEEE Antennas and Propagation Society International Symposium. 1996 Digest*, Vol. 1, 684–687, Baltimore, MD, USA, 1996.

[59] Xu, H., J. Cui, J. Duan, B. Zhang, and Y. Tian, "Versatile conical conformal array antenna based on implementation of independent and endfire radiation for UAV applications," *IEEE Access*, Vol. 7, 31 207–31 217, 2019.

[60] Volakis, J. L., *Antenna Engineering Handbook*, 4th ed., McGraw-Hill, New York, 2007.

[61] Gabriel, C., "Compilation of the dielectric properties of body tissues at RF and microwave frequencies," *Brooks Air Force Technical Report*, AL/OE-TR-1996-0037, 1996.

[62] IEC/IEEE P62704-3/D4, "Approved Draft International Standard: Determining the peak spatial-average specific absorption rate (SAR) in the human body from wireless communication devices, 30 MHz-6 GHz — Part 3: Specific requirements for using the finite-difference time-domain (FDTD) method for SAR calculations of mobile phones," IEC/IEEE, 2017.

[63] International Commission on Non-Ionizing Radiation Protection (ICNIRP), "Guidelines for limiting exposure to electromagnetic fields (100 kHz to 300 GHz)," *Health Physics*, Vol. 118, No. 5, 483–524, 2020.

[64] IEEE Std C95.1-2019, "Safety levels with respect to human exposure to electric, magnetic, and electromagnetic fields (0 Hz-300 GHz)," IEEE, New York, USA, 2019.